Chapter 6

Porous Truncated Cone Squeeze Film-Bearing with Different Porous Structures

Contents

6.1 Introduction

As discussed earlier in Chapter 5, the fluid film between two surfaces with a relative normal velocity is important in many frictional devices in industry as well as in human body. This Chapter studied squeeze film geometry of truncated cone. Prakash and Vij [1] analyzed lower porous plate squeeze film bearing of different shapes (annular, circular, elliptic, rectangular and cone) using Morgan-Cameron approximation. The effects of the shape of plate and porosity on the bearing performance are calculated. Kumar *et. al.* [2] studied ferrofluid based squeeze film for spherical and conical bearings. The magnetic field considered was in the transverse direction of the fluid flow. Here, they have considered Shliomis model to solve the problem because it taken care of rotation of the fluid particles as well as liquid. The resulting governing equations are nonlinear coupled equations and are solved using perturbation method in terms of dimensionless Brownian relaxation time parameter. The effect of magnetic fluid parameters on various bearing characteristics is studied numerically. Prajapati [3] analyzed various designed bearings like circular, annular, elliptic, conical, etc. It is shown that with the increase of magnetization parameter «*, the load carrying capacity increases. Thus, concluded the superiority performance of the bearings with MF as lubricant. It is also concluded that the bearing with MF can support a load even when there is no flow. Patel and Deheri [4] studied squeeze film based on magnetic fluid for conical plates. There they found that the performance of the bearing with this lubricant is relatively better than the conventional lubricant. Also, it is found that the negative effect induced buy the porosity can be neutralize by the positive effect caused by the magnetization parameter. Further, the paper suggests about the choosing of suitable combination of the magnetization parameter and semi-vertical angle for enhancing bearing performances. Vadher *et. al.* [5] analyzed performance of hydromagnetic squeeze film

between two conducting truncated conical plates. The plates are considered electrically conducting and the clearance space between them is filled by an electrically conducting lubricant. A uniform transverse magnetic field is applied between the plates. The resulting Reynolds equation is solved for pressure, load carrying capacity and response time. The results suggest better performances for the bearing as compared to conventional lubricant. Andharia and Deheri [6] studied longitudinal roughness effect on MF based squeeze film between conical plates. It is shown that the performance of the bearing gets enhanced due to negative skewed roughness. Also, it is shown that the standard deviation increases the load carrying capacity which is unlike the case of transverse surface roughness. Recently, Lin *et. al.* [7] studied effects of fluid inertia forces on the squeeze film characteristics of conical plates using ferrofluid lubricant. By applying the averaged momentum principle, a lubrication equation governing the film pressure is derived. Comparing with the non-inertia non-magnetic case, better squeeze performances are predicted when operating with large value of the inertial parameter of fluid inertia forces.

This Chapter studied porous truncated cone squeeze film-bearing model considering the effects of porosity, permeability, squeeze velocity and oblique variable magnetic field. Effects of two permeability models-globular sphere and capillary fissures are also discussed. Expressions for pressure and load carrying capacity are obtained. The results for dimensionless load carrying capacity are computed.

6.2 Mathematical Formulation of Globular Sphere - Permeability Model

Figure 6.1 shows schematic diagram of porous truncated cone squezee film-bearing. The lower surface is attached with a porous matrix of thickness H^*.

By the usual assumptions of lubrication theory, neglecting inertia terms, derivatives of fluid velocity across the film predominate and combining equations (2.18) to (2.22), the equation governing the pressure distribution p in the film region using ferrofluid (FF) as lubricant satisfies the modified equation [8, 9]

$$\frac{\partial}{\partial x}\left[h^3\frac{\partial}{\partial x}\left(p-\frac{1}{2}\mu_0\overline{\chi}H^2\right)\right]+\frac{\partial}{\partial y}\left[h^3\frac{\partial}{\partial y}\left(p-\frac{1}{2}\mu_0\overline{\chi}H^2\right)\right]=12\eta\dot{h}-12\eta w\big|_{z=0},$$

… (6.1)

with

$$\frac{\partial^2}{\partial x^2}\left(P-\frac{1}{2}\mu_0\overline{\chi}H^2\right)+\frac{\partial^2}{\partial y^2}\left(P-\frac{1}{2}\mu_0\overline{\chi}H^2\right)+\frac{\partial^2}{\partial z^2}\left(P-\frac{1}{2}\mu_0\overline{\chi}H^2\right)=0.$$

… (6.2)

where x, y, z are the Cartesian coordinates, h is the film thickness, H is strength of variable magnetic field, $\dot{h}=dh/dt$ is the squeeze velocity of the upper bearing surface, w_0 is the z-component of the fluid velocity at $z = 0$, η is fluid viscosity, μ_0 is the free space permeability, $\overline{\chi}$ is magnetic susceptibility and P is pressure in the porous region.

Integrating equation (6.2) with respect to z over the porous matrix thickness $(-H^*, 0)$ yields

$$\left[\frac{\partial}{\partial z}\left(P-\frac{1}{2}\mu_0\overline{\chi}H^2\right)\right]_{z=-H^*}^{z=0}=-\int_{-H^*}^{0}\left[\frac{\partial^2}{\partial x^2}\left(P-\frac{1}{2}\mu_0\overline{\chi}H^2\right)+\frac{\partial^2}{\partial y^2}\left(P-\frac{1}{2}\mu_0\overline{\chi}H^2\right)\right]dz.$$

… (6.3)

Since

$$\left[\frac{\partial}{\partial z}\left(P-\frac{1}{2}\ll_0\overline{\ll}H^2\right)\right]_{z=-H^*}=0\,,$$

… (6.4)

as $z=-H^*$ is a solid surface, that is the porous matrix is press-fitted with a solid housing as shown in Figure 6.1.

Using equations (6.3) and (6.4)

$$\left[\frac{\partial}{\partial z}\left(P-\frac{1}{2}\ll_0\overline{\ll}H^2\right)\right]_{z=0}\approx -H^*\left[\frac{\partial^2}{\partial x^2}\left(p-\frac{1}{2}\ll_0\overline{\ll}H^2\right)+\frac{\partial^2}{\partial y^2}\left(p-\frac{1}{2}\ll_0\overline{\ll}H^2\right)\right],$$

… (6.5)

using Morgan-Cameron approximation [8].

Using Darcy's law, the z -component of velocity in the porous region is given by

$$\overline{w}\big|_{z=0}=-\frac{£^3 D_c^2}{180\,(1-£)^2\,¦}\left[\frac{\partial}{\partial z}\left(P-\frac{1}{2}\ll_0\overline{\ll}H^2\right)\right]_{z=0},$$

… (6.6)

where D_c is a mean particle size, £ is the porosity of the porous matrix (refer Figure 6.2).

Assuming the normal components of velocity across the film-porous interface is continuous, therefore $w\big|_{z=0}=\overline{w}\big|_{z=0}$, which yields, using equations (6.1), (6.5) and (6.6) as

$$\frac{\partial}{\partial x}\left[h^3\frac{\partial}{\partial x}\left(p-\frac{1}{2}\rho_0\bar{\omega}H^2\right)\right]+\frac{\partial}{\partial y}\left[h^3\frac{\partial}{\partial y}\left(p-\frac{1}{2}\rho_0\bar{\omega}H^2\right)\right]$$
$$=12\eta\dot{h}-\frac{\varepsilon^3 D_c^2}{15(1-\varepsilon)^2}H^*\left[\frac{\partial^2}{\partial x^2}\left(p-\frac{1}{2}\rho_0\bar{\omega}H^2\right)+\frac{\partial^2}{\partial y^2}\left(p-\frac{1}{2}\rho_0\bar{\omega}H^2\right)\right],$$

… (6.7)

implies

$$\left[h^3+\frac{\varepsilon^3 D_c^2}{15(1-\varepsilon)^2}H^*\right]\left[\frac{\partial^2}{\partial x^2}\left(p-\frac{1}{2}\rho_0\bar{\omega}H^2\right)+\frac{\partial^2}{\partial y^2}\left(p-\frac{1}{2}\rho_0\bar{\omega}H^2\right)\right]=12\eta\dot{h}$$

… (6.8)

or

$$\nabla^2\left(p-\frac{1}{2}\rho_0\bar{\omega}H^2\right)=\frac{12\eta\dot{h}}{\left[h^3+\frac{\varepsilon^3 D_c^2}{15(1-\varepsilon)^2}H^*\right]},$$

… (6.9)

Using equation (6.9) and referring literature [1, 4], the Reynolds-type equation for the film pressure can be obtained as

$$\frac{1}{x}\frac{d}{dx}\left[x\frac{d}{dx}\left(p-\frac{1}{2}\rho_0\bar{\omega}H^2\right)\right]=\frac{12\eta\dot{h}\sin\mu}{\left(h^3\sin^3\mu+\frac{\varepsilon^3 D_c^2}{15(1-\varepsilon)^2}H^*\right)},$$

… (6.10)

where μ is the semi-vertical angle of the truncated cone.

Using equation (6.10) and choosing oblique and variable magnetic field [6]

$$H^2 = K(a\,\mathrm{cosec}\,\mu - x)(x - b\,\mathrm{cosec}\,\mu),$$

… (6.11)

where K is chosen to suit the dimension of both sides, a is upper radius of the truncated cone and b is the lower radius of the truncated cone, the concerned Reynolds-type equation for the film pressure can be obtained as

$$\frac{1}{x}\frac{d}{dx}\left\{x\frac{d}{dx}\left[p - \frac{1}{2}\,«_0\,\bar{«}K(a\,\mathrm{cosec}\,\mu - x)(x - b\,\mathrm{cosec}\,\mu)\right]\right\} = \frac{12\,¦\,\dot{h}\sin\mu}{\left(h^3\sin^3\mu + \frac{£^3 D_c^2}{15\,(1-£)^2}H^*\right)}.$$

… (6.12)

Using boundary conditions

$$p(a\,\mathrm{cosec}\,\mu) = 0 \text{ and } p(b\,\mathrm{cosec}\,\mu) = 0,$$

… (6.13)

equation (6.12) becomes

$$p = \frac{1}{2}\,«_0\,\bar{«}K(a\,\mathrm{cosec}\,\mu - x)(x - b\,\mathrm{cosec}\,\mu) + \frac{3\,¦\,\dot{h}\,\mathrm{cosec}\,\mu\,(a^2 - b^2)}{\left(h^3\sin^3\mu + \frac{£^3 D_c^2}{15\,(1-£)^2}H^*\right)}\left[\frac{\frac{x^2\sin^2\mu}{b^2} - 1}{(a/b)^2 - 1} - \frac{\ln\left(\frac{x\sin\mu}{b}\right)}{\ln(a/b)}\right],$$

… (6.14)

which can be written in dimensionless form as

$$\overline{p} = -\frac{ph^3}{\dot{h}(a^2-b^2)\operatorname{cosec}\mu} = \frac{«*}{2(a^2-b^2)}\frac{(a\operatorname{cosec}\mu - x)(x - b\operatorname{cosec}\mu)}{\operatorname{cosec}\mu} + \frac{3}{\left(\sin^3\mu + \frac{£^3}{15(1-£)^2}\cdot\right)}\left[\frac{\ln\left(\frac{x\sin\mu}{b}\right)}{\ln(a/b)} - \frac{\left(\frac{x^2\sin^2\mu}{b^2}-1\right)}{(a/b)^2-1}\right],$$

… (6.15)

where

$$«* = -\frac{«_0\overline{«}Kh^3}{\dot{h}},\quad \cdot\ = \frac{D_c^2\,H*}{h^3}.$$

… (6.16)

6.3 Calculation of Load Carrying Capacity

The definition of load carrying capacity

$$W = 2® \int_{b\operatorname{cosec}\mu}^{a\operatorname{cosec}\mu} px\,dx,$$

… (6.17)

implies

$$W = \frac{\pi \alpha_0 \bar{\alpha} K (a^2 - b^2)^2 \operatorname{cosec}^4 \mu}{12} \left[\frac{(a/b)^2 + 1}{(a/b)^2 - 1} - \frac{2(a/b)}{(a/b)^2 - 1} \right] - \frac{3\pi \dot{h} \operatorname{cosec}^3 \mu \, (a^2 - b^2)^2}{2\left(h^3 \sin^3 \mu + \frac{\varepsilon^3 D_c^2}{15 (1-\varepsilon)^2} H^* \right)} \left[\frac{(a/b)^2 + 1}{(a/b)^2 - 1} - \frac{1}{\ln(a/b)} \right],$$

... (6.18)

which can be written in dimensionless form as

$$\bar{W} = -\frac{Wh^3}{\eta \dot{h} \pi^2 (a^2 - b^2)^2 \operatorname{cosec}^4 \mu} = \frac{\alpha^*}{12\pi} \left[\frac{(a/b)^2 + 1}{(a/b)^2 - 1} - \frac{2(a/b)}{(a/b)^2 - 1} \right] + \frac{3 \operatorname{cosec}^2 \mu}{2\pi \left(1 + \frac{\varepsilon^3}{15 (1-\varepsilon)^2} \cdot \operatorname{cosec}^3 \mu \right)} \left[\frac{(a/b)^2 + 1}{(a/b)^2 - 1} - \frac{1}{\ln(a/b)} \right],$$

... (6.19)

where α^* and $\cdot$ are defined as in equation (6.16).

6.4 Mathematical Formulation of Capillary Fissures - Permeability Model

When the porous matrix is designed with capillary fissures composed of three sets of mutually orthogonal fissures as suggested by Irmay [6], then equation (6.9) becomes

$$\nabla^2 \left(p - \frac{1}{2} \alpha_0 \bar{\alpha} H^2 \right) = \frac{12 \eta m \dot{h}}{m h^3 + (1 - m^{\frac{2}{3}})(1 - m^{\frac{1}{3}})^2 D_s^2 H^*},$$

... (6.20)

where D_s is a mean solid size and $m = 1 - \varepsilon = \dfrac{a^3}{(a+b)^3}$ (refer Figure 6.3).

The load carrying capacity in dimensionless form can be obtained as

$$\bar{W} = -\frac{Wh^3}{\dot{h}\mu^2(a^2-b^2)^2\,\mathrm{cosec}^4\alpha} = \frac{\beta^*}{12\mu}\left[\frac{(a/b)^2+1}{(a/b)^2-1} - \frac{2(a/b)}{(a/b)^2-1}\right]$$

$$+\frac{3\,\mathrm{cosec}^2\alpha}{2\mu\left(1+\dfrac{(1-m^{\frac{2}{3}})(1-m^{\frac{1}{3}})^2}{m}\cdot\,\mathrm{cosec}^3\alpha\right)}\left[\frac{(a/b)^2+1}{(a/b)^2-1} - \frac{1}{\ln(a/b)}\right], \quad \text{... (6.21)}$$

where

$$\beta^* = -\frac{\beta_0\bar{\beta}Kh^3}{\dot{h}}, \quad \gamma = \gamma_f = \frac{D_s^2 H^*}{h^3}. \quad \text{... (6.22)}$$

6.5 Results and Discussion

Table 6.1 shows the results of $\bar{W}$ for porous truncated cone squeeze film-bearing considering $\bar{W} = -Wh^3/\dot{h}\mu^2(a^2-b^2)^2\,\mathrm{cosec}^4\alpha$.

It is observed from the table that porous truncated cone does not support load when dimensionless magnetization parameter $\beta^* = 0$ and dimensionless permeability parameter $\gamma = 0.0001$, that is when there is no use of FF as lubricant. But when FF is used as lubricant, then it supports load and this effect is more evident as β^* increases. Moreover, the reverse trend of $\bar{W}$ is observed with respect to γ, that is as compared to other previous bearing designs here $\bar{W}$ increases with the increase of γ.

6.5.1 Comparison between globular sphere and capillary fissures models of truncated cone with other bearing designs

When the porous matrix is designed with globular spheres suggested by Kozeny-Carman [10], then the permeability of the porous matrix attached at the lower plate or disk is defined by

$$\frac{£^3 D_c^2}{180\,(1-£)^2},$$

where D_c is a mean particle size, £ is the porosity of the porous matrix.

When the porous matrix designed with capillary fissures composed of three sets of mutually orthogonal fissures as suggested by Irmay [10], then the permeability of the porous matrix attached at the lower plate is defined by

$$\frac{(1-m^{\frac{2}{3}})(1-m^{\frac{1}{3}})^2 D_s^2}{12m},$$

where D_s is a mean solid size and $m = 1-£ = \frac{a^3}{(a+b)^3}$. The impact of these two porous structures on $\bar{W}$ is shown in Table 6.2 [11] for the following value of different parameters.

$$£ = 0.2\,, D_c = D_s = 0.00001(\text{m}),\ H^* = 0.0001(\text{m}),$$
$$h = 0.000005(\text{m}),\ \mu = ® / 6\ (rad.).$$

From the Table 6.2, it is observed that better load carrying capacity can be obtained when the porous matrix is designed with globular porous structures except for truncated cone bearing design system. For truncated cone bearing design system capillary fissures structures have better effect on $\bar{W}$.

6.6 Conclusions

Reynolds-type equation for squeeze film-bearing truncated cone design system is theoretically derived by considering equations from ferrohydrodynamic theory by R.E. Rosensweig and equation of continuity in film as well as porous region. The validity of the Darcy's law is assumed in the porous region. The effects of porosity, permeability, squeeze velocity and variable magnetic field are considered. The variable magnetic field considered here is oblique to the lower disk or plate. Moreover, the porous surface is considered because of its advantageous property of self-lubrication and no need of exterior lubricant supply.

It is concluded that the porous truncated cone bearing does not support load in the case of conventional lubricant, whereas it does in the case of FF as lubricant for smaller values of $\cdot$. Moreover, the reverse trend of $\bar{W}$ can be observed with respect to $\cdot$ as compared to other bearing design systems. Moreover, the better performance (in the sense of $\bar{W}$ increases) of the bearings are observed in the case of globular sphere model suggested by Kozeny-Carman for permeability in the porous region except in the case of truncated cone bearing design, where better load carrying capacity can be obtained in the case of capillary fissures model.

6.7 Figures

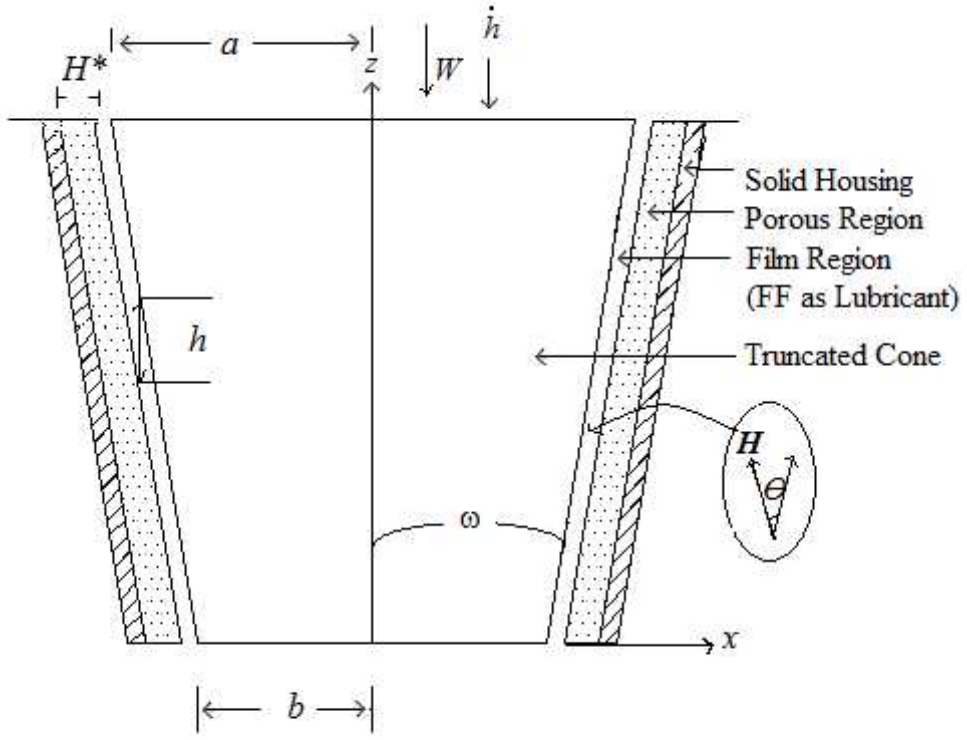

Figure 6.1 Schematic diagram of porous truncated cone squeeze film geometry.

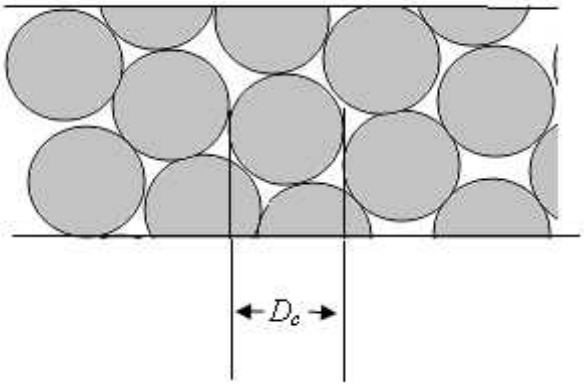

Figure 6.2 Globular sphere model of porous matrix suggested by Kozeny-Carman.

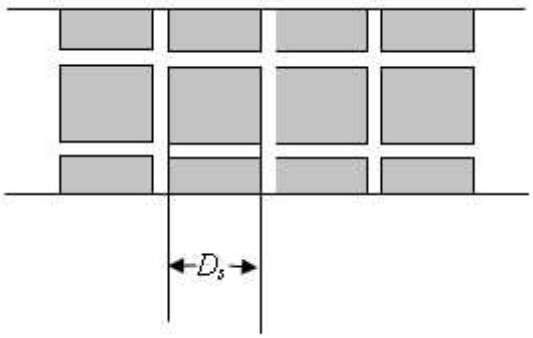

Figure 6.3 Capillary fissures model of porous matrix suggested by Irmay.

6.8 Tables

Dimensionless permeability parameter	$\bar{W}$		
	«* = 0	«* = 0.2	«* = 0.3
· = 0.0001	0.00000	0.01745	0.02618
· = 0.01	0.00003	0.01749	0.02622
· = 1.0	0.19970	0.21716	0.22588

Table 6.1 Comparison of dimensionless load carrying capacity $\bar{W}$ for $\mu = ® / 6$.

Bearing geometry	$\bar{W}$				
	Annular	Circular	Infinitely long rectangular $(a < b)$	Complete cone	Truncated cone
Globular sphere model	9.1364	4.4628	1.9241	12.2885	0.0262
Capillary fissures model	0.8765	0.3650	0.1849	0.1984	0.2469

Table 6.2 Comparison between globular sphere model and capillary fissures model.

6.9 References

[1] Prakash J and Vij S K, Load capacity and time-height relations for squeeze films between porous plates, *Wear*, 24, 309-322 (1973).

[2] Kumar D, Sinha P and Chandra P, Ferrofluid squeeze film for spherical and conical bearings, *International Journal of Engineering Science*, 30(5), 645-656 (1992).

[3] Prajapati B L, Magnetic-fluid-based porous squeeze films, *Journal of Magnetism and Magnetic Materials*, 149, 97-100 (1995).

[4] Patel R M and Deheri G M, Magnetic fluid based squeeze film between porous conical plates, *Industrial Lubrication and Tribology*, 59(3), 143-147 (2007).

[5] Vadher P A, Deheri G M and Patel R M, A study on the performance of hydromagnetic squeeze film between two conducting truncated conical plates, *Jordan Journal of Mechanical and Industrial Engineering*, 2(2), 85-92 (2008).

[6] Andharia P I and Deheri G M, Effect of longitudinal roughness on magnetic fluid based squeeze film between truncated conical plates, *FDMP*, 7(1), 111-124 (2011).

[7] Lin J R, Lin M C, Hung T C and Wang P Y, Effects of fluid inertia forces on the squeeze film characteristics of conical plates-ferromagnetic fluid model, *Lubrication Science*, 25, 429 - 439 (2013).

[8] Shah R C and Bhat M V, Ferrofluid lubrication equation for porous bearings considering anisotropic permeability and slip velocity, *Indian Journal of Engineering and Materials Sciences*, 10, 277-281 (2003).

[9] Morgan V T and Cameron A, The mechanism of lubrication in porous metal bearings, *Proc Conf on Lubrication and Wear, Institute of Mechanical Engineers*, 151-157 (1957).

[10] Liu J, Analysis of a porous elastic sheet damper with a magnetic fluid, *Journal of Tribology*, 131, 0218011-15 (2009).

[11] Shah R C, Patel N I and Kataria R C, Some porous squeeze film-bearings using ferrofluid lubricant: A review with contributions, *Journal of Engineering Tribology*, 230(9), 1157-1171 (2016).